Supplement of Atmos. Chem. Phys., 23, 8531–8551, 2023
https://doi.org/10.5194/acp-23-8531-2023-supplement

Atmospheric Chemistry and Physics Open Access

Supplement of

Estimating nitrogen and sulfur deposition across China during 2005 to 2020 based on multiple statistical models

Kaiyue Zhou et al.

Correspondence to: Yu Zhao (yuzhao@nju.edu.cn)

Number of tables:9 Number of figures: 5

Table list

Table S1. Social-economical and geo-climatic conditions for six regions of China.

Table S2. Input variables in the RF algorithm.

Table S3. The modeled V_d for different land use categories (cm s^{-1}).

Table S4. Comparison of the annual F_d of N and S in this and other studies (kg N/S ha^{-1} yr^{-1}).

Table S5. The Mann-Kendall trend test trend analysis of the $R_{dry/wet}$ of N and S in 2005-2020. The z-value represents the standard normal statistic, and the p-value represents the generalization. The z-value represents the trend direction, while the p-value represents whether there is a statistically significant level. P1 and P2 indicate 2005–2015 and 2015–2020, respectively.

Table S6. Comparisons of total deposition fluxes of different species between our study in China and two networks in other countries (kg N/S ha^{-1} yr^{-1}).

Table S7. The ratios of deposition of different forms and species for the six regions as well as eastern (SE+NC with Inner Mongolia excluded), western (NW+TP), and whole China.

Table S8. The annual emissions, deposition, and D/E by land use type, according to the latest Land-Use and Land-Cover Change (LUCC) information (http://www.resdc.cn/). “Urban” includes city/town and building categories, and “Rural” includes cropland and countryside categories.

Table S9 in the revised supplement: Comparison of the annual V_d of nitrogen compounds by land use type in this and other studies (cm s^{-1}).

Figure list

TEXT SECTION: THE RF ALGORITHM AND EVALUATION

Basic algorithm of RF model

Decision tree (*tree*) is a basic classification and regression prediction model. It presents a tree structure that uses sample features as criteria and values as branches.

For *tree* = 1 to 1000:

- ✧ The samples and characteristic variables are randomly selected by the method of sampling with return (Liaw and Wiener, 2002);
- ✧ The best partition features and eigenvalues are found by minimizing the square error between the observation value and the mean value;
- ✧ The final output value of the base decision tree is obtained by the mean value of the response variables.

The model output is the average of the predictions of all trees.

The algorithm of RF regression model consists of a set of regression subtrees to form a set of combination models (Breiman, 2001), as expressed in Eq. (S1):

$$\bar{h}(x) = \frac{1}{N}\sum_{n=1}^{N}\{h(x_{\mathrm{k}}, \theta_{\mathrm{n}})\} \quad \text{(S1)}$$

where $h(x_{\mathrm{k}}, \theta_{\mathrm{n}})$ denotes the base decision tree of random forest; θ_n denotes a random vector with independent and identically distribution; x_k denotes an interpretation variable.

The best partition features *j* and eigenvalues *s* are determined by the square error minimization criterion, as expressed in Eq. (2) (Li et al., 2020):

$$\min_{j,s}[\min_{c_1}\sum_{xi\in R_1(j,s)}(y_i - c_1)^2 + \min_{c_2}\sum_{xi\in R_2(j,s)}(y_i - c_2)^2] \quad \text{(S2)}$$

The *min* of inner layer is the minimum value selected by each feature at its own feature level, i.e., the best partition feature point is selected for each feature; and the outer layer *min* is the selected feature with the smallest error at each feature level. R_1 and R_2 denote the two regions divided by partition condition (the eigenvalue *s* of feature *j* is the logical judgment condition).

The model traverses all the characteristic variables *j*, scans the segmentation point *s* for the fixed partition variable, and selects the pair (*j*, *s*) that makes the Eq. (S2) reach the minimum value.

Determination of the relative importance of interpretation variables (RIV)

The idea of using RF to evaluate the RIV (dimensionless) is to see how much contribution of each feature has made to each tree, and finally we compare the contribution between features (Grömping, 2009; Wei et al., 2019). Conventional RIV calculation methods are divided into two types, i.e., calculated based on Gini index (RIV_j^{Gini}) and out-of-bag (OOB) data error rate (RIV_j^{OOB}).

(1) Calculation based on Gini index(RIV_j^{Gini}).

The calculation based on Gini index (*GI*) is expressed in Eq. (S3):

$$GI_m = \sum_{k=1}^{K} \hat{p}(1-\hat{p}) \tag{S3}$$

where *K* denotes the number of the features; $\hat{p}$ denotes the probability estimation value of node *m* sample belonging to class *K*.

The RIV to variable X_j on the node *m*, i.e., the Gini index change before and after node *m* branching, can be determined in Eq. (S4):

$$RIV_{jm}^{Gini} = GI_m - GI_l - GI_r \tag{S4}$$

where GI_l and GI_r denote the Gini index of two new nodes after *m* node splitting.

The final RIV is calculated with Eq. (S5):

$$RIV_j^{Gini} = \frac{1}{n}\sum_{i=1}^{n} RIV_{jm}^{Gini} \tag{S5}$$

(2) Calculation based on the OOB error rate (RIV_j^{OOB}).

✧ In each tree of RF, the training self-service samples are randomly selected to build the tree, and the prediction error rate of the out of bag data (OOB) is calculated.

✧ The observation value of the variable X_j is randomly replaced, and the prediction error rate of OOB is calculated again.

✧ Finally, the difference between the two OOB error rates is calculated.

After standardization, the mean value in all trees is the RIV_j^{OOB} of variable X_j.

Introduction to the calculation of V_d for all N and S species

The dry deposition flux of gaseous and particulate N and S species was calculated by multiplying measured concentrations with simulated V_d from the GEOS (Goddard Earth Observing System)-Chem chemical transport model (http://geos-chem.org). The model calculation of V_d follows a standard big-leaf resistance-in-series model as described by Wesely (1989) for gases and Zhang et al. (2001) for aerosol.

For gases N and S compounds, the V_d is calculated as the reciprocal of three serially connected resistances:

$$V_d = \frac{1}{R_a+R_b+R_c} \quad \text{(S6)}$$

where R_a is aerodynamic resistance of underlying surface, which refers to the air resistance experienced by the gas from the atmosphere to the surface turbulent motion (same value for both species, Hicks et al., 1987); R_b is the quasi-laminar boundary layer resistance, which refers to the resistance of the gas from the quasi-laminar boundary layer to the near ground (Walcek et al., 1986); and R_c is the surface resistance, which refers to the resistance of gas molecules absorbed by the surface.

For aerosol, V_d is governed by interception, inertial and gravitational forces. It is computed by:

$$V_d = \frac{1}{R_a+R_b+R_aR_bV_g} + V_g \quad \text{(S7)}$$

where V_g is the gravitational settling velocity (Zhang et al., 2001).

The R_a and R_b to turbulent transfer from the measurement heights (~3 m) to the roughness height is estimated using the MERRA-2 data. The R_c is calculated based on the Global Land Cover Characteristics Data Base Version 2.0 (http://edc2.usgs.gov/glcc/globdoc2_0.php), which defines land types (e.g., urban, forest, etc.) at 1 km × 1 km resolution and is then binned to the model resolution as fraction of the grid cell covered by each land type. Bi-directional NH_3 exchange is not considered in the model. Then, the monthly V_d was averaged based on the

hourly dataset for further estimation of dry deposition flux of each N and S species, which was statistically summarized according to land use type and is presented in Table S3.

Table S1. Social-economical and geo-climatic conditions for six regions of China.

Regions	The percentage of China		Climatic conditions
	Area	GDP	
NC	10%	28%	temperate monsoon climate
NE	6%	9%	temperate monsoon climate
NW	35%	5%	temperate continental climate
SE	13%	46%	subtropical monsoon climate
SW	14%	12%	subtropical and plateau monsoon climates
TP	20%	0.5%	alpine mountain climate

Table S2. Input variables in the RF algorithm.

Class	Symbol	Description
Response variable	F_d	Observed ground-level concentration×modeled V_d, kg N/S ha^{-1} yr^{-1}
Interpretation variables		
Satellite-derived VCD	SAT	Satellite-derived vertical columns densities, 10^{15}mol cm^{-2}
Meteorology	sp	Surface pressure
	wind	Wind direction, °
	t2m	Temperature at 2 meters, K
	pre	Precipitation, mm
	si10	Wind speed at 10 meters, m s^{-1}
	blh	Boundary layer height, m
	tcw	Total column water, kg m^{-2}
	tclw	Total column liquid water, kg m^{-2}
	d2m	Dewpoint temperature at 2 meters, K
	tco3	Total column ozone, kg m^{-2}
	kx	K index, K
	zust	Friction velocity, m s^{-1}
	gwd	Gravity wave dissipation, J m^{-2}
	tcc	Total cloud cover
	bld	Boundary layer dissipation, J m^{-2}
	magss	Magnitude of turbulent surface stress, N m^{-2} s
Emissions	eNOX	Emission of NO_X, Mg $grid^{-1}$
	eNH3	Emission of NH_3, Mg $grid^{-1}$
	eSO2	Emission of SO_2, Mg $grid^{-1}$
Geography	Lai_lv	Leaf area index, low vegetation, m^2 m^{-2}
	lai_hv	Leaf area index, high vegetation, m^2 m^{-2}
	ROAD	Road density, km $grid^{-1}$
	DEM	Elevation, m
	LUCC	Land use type proportion, %
	GDP	Gross Domestic Product, 10000 yuan km^{-2}
	POP	Population density, people km^{-2}
Modeled concentrations from CTM	c_species	Including HNO_3, NH_3, NH_4^+, NO_3^-, SO_4^{2-}, ug m^{-3}

Table S3. The modeled V_d for different land use categories (cm s^{-1}).

Land use category	HNO_3	NH_3	NH_4	NO_2	NO_3	SO_2	SO_4
Paddy fields	1.63	0.47	0.14	0.20	0.14	0.45	0.14
Dry land	1.42	0.42	0.16	0.17	0.16	0.41	0.16
Forestland	2.55	0.49	0.14	0.24	0.14	0.46	0.14
Shrub forest	1.83	0.45	0.16	0.21	0.16	0.43	0.16
Sparse forestland	1.96	0.47	0.15	0.22	0.15	0.44	0.15
Other forestland	2.17	0.53	0.14	0.22	0.14	0.52	0.14
High coverage grassland	1.29	0.36	0.18	0.12	0.18	0.36	0.18
Medium coverage grassland	1.05	0.34	0.18	0.09	0.18	0.34	0.18
Low coverage grassland	0.88	0.31	0.17	0.04	0.17	0.31	0.17
River channel	1.17	0.38	0.15	0.13	0.15	0.37	0.15
Lakes	0.93	0.32	0.19	0.07	0.19	0.32	0.19
Reservoir pond	1.37	0.43	0.14	0.14	0.14	0.43	0.14
Permanent glacial snow	0.59	0.27	0.16	0.03	0.16	0.28	0.16
Tidal-flat	1.06	1.01	0.07	0.02	0.07	1.02	0.07
Beach land	1.30	0.37	0.16	0.12	0.16	0.36	0.16
Urban land use	1.37	0.44	0.15	0.14	0.15	0.44	0.15
Rural settlements	1.27	0.40	0.15	0.14	0.15	0.40	0.15
Other construction land	1.40	0.47	0.14	0.16	0.14	0.47	0.14
Sand	0.87	0.30	0.10	0.02	0.10	0.30	0.10
Gobi	0.98	0.30	0.10	0.02	0.10	0.30	0.10
Saline alkali soil	0.87	0.31	0.15	0.04	0.15	0.31	0.15
Swamp land	1.61	0.38	0.15	0.14	0.15	0.37	0.15
Bare land	1.10	0.30	0.10	0.03	0.10	0.30	0.10
Bare rock	0.88	0.30	0.14	0.03	0.14	0.30	0.14
Other unused land	0.72	0.29	0.18	0.04	0.18	0.30	0.18

Note: Land-Use and Land-Cover Change (LUCC) data were obtained from Resource and Environment Data Cloud Platform (http://www.resdc.cn/), generated by manual visual interpretation of Landsat TM/ETM remote sensing images.

Table S4. Comparison of the annual F_d of N and S in this and other studies (kg N/S ha^{-1} yr^{-1}).

Reference	Study region	Research scale	Study period	Dry deposition							Wet/bulk deposition			Total deposition	
				NO_2	HNO_3	NO_3^-	NH_3	NH_4^+	SO_2	SO_4^{2-}	NH_4^+	NO_3^-	SO_4^{2-}	N	S
This study	China	Grid level	2005-2020	3.4	5.3	1.7	10.3	4.2	15.5	1.2	3.3	4.6	6.4	32.9	23.1
Nowlan et al. (2014)	China	Grid level	2005-2007	0.2											
Lye and Tian (2007)	China	Grid level	2003	2.9							7.1	2.8		12.9	
Jia et al. (2014)	China	Grid level	1980-2010												
Jia et al. (2016)	China	Grid level	2005-2014	0.6	1.1	0.1	5.4	0.3				13.9			
Tan et al. (2022)	China	Grid level	2010								4.2	3.4			
Itahashi et al. (2018)	China	Grid level	2010								3.5	2.5			
Zhao et al. (2017)	China	Grid level	2008-2012	0.3	1.7	1.0	0.5	2.6			6.6	3.4		18.1	
Xu et al. (2015)	China	43 sites	2010-2014	0.2-9.8	0.2-16.6	0.1-4.5	0.5-16.0	0.1-11.7			1.0-19.1	0.5-20.1		39.9	
Xu et al. (2019)	China	32 sites	2010-2015	3.1	5.2	1.4	9.6	3.7			11.4	10.3			
Wen et al. (2020)	China	66 sites	2011-2018			22.5						19.4			
Pan et al. (2012)	North China	10 sites	2007-2010	0.8-4.5		2.2-3.1	8.1-64.2	1.7-5.5			10.3-22.0	3.4-10.2		60.6	
Pan et al. (2013)	North China	10 sites	2007-2010						32.4	12.8			19.6		64.8
Zhu et al. (2015)	China	Grid level	2013								7.3	5.9			
Yu et al. (2016)	China	43 sites	2009-2014									32.9	116.0		
Yu et al. (2019)	China	Grid level	1985-2015	0.8	2.0	2.7	0.5	4.3			5.9	4.2		20.4	
Li et al. (2019)	China	Grid level	2010										71.5		
Li et al. (2020)	China	Grid level	2011-2016								5.9	13.3	33.4		
Liu et al. (2016a)	Southwest China	1 site	2003-2013								17.5	8.2	21.7		
Liu et al. (2016b)	China	225 data records	2003-2014								6.8	5.4			
Liu et al. (2016c)	China	174 sites	2000-2013										23.0		
Liu et al. (2017a)	China	Grid level	2010-2012									5.8			

Table S4 (continued)

Reference	Study region	Research scale	Study period	Dry deposition							Wet/bulk deposition			Total deposition	
				NO_2	HNO_3	NO_3^-	NH_3	NH_4^+	SO_2	SO_4^{2-}	NH_4^+	NO_3^-	SO_4^{2-}	N	S
Liu et al. (2017b)	China	Grid level	2012			1.5									
Liu et al. (2021)	China	Grid level	2008-2016								6.5				
Luo et al. (2016)	China	16 sites	2010-2012						2.3-26.5	0.5-3.4					
Ge et al. (2014)	China	Grid level	2007								9.1	9.1	48.8	35.0	83.3
Kuribayashi et al. (2012)	China	6 sites	2001-2005						23.5	3.8				49.4	
Zhang et al. (2017)	China	Grid level	2007-2014	0.005-8.54											
Zhou et al. (2021)	China	Grid level	2013-2018	2.1-3.1					7.5-18.4						
Qiao et al. (2015a)	Sichuan, China	1 site	2010-2011								1.4	1.3	8.1		
Qiao et al. (2015b)	Sichuan, China	Grid level	2010-2011									0.3	2.8		
Zhang et al. (2022)	Tibetan Plateau	27 sites													
Larssen et al. (2011)	South China	4 sites	2001-2004								0.4-0.9	0.2-0.5	0.9-1.9	0.4-2.5	1.5-10.5
Jiang et al. (2020)	Hunan, China	5 sites	2015-2016						8.6				18.2		26.8

Table S5. The Mann-Kendall test for the trend of $R_{dry/wet}$ of N and S in 2005-2020. The z-value represents the standard normal statistic, and the p-value represents the generalization. The former indicates the trend, while the latter indicates statistical significance. P1 and P2 indicate 2005–2015 and 2015–2020, respectively.

Species	OXN		RDN		N		S	
Period	P1	P2	P1	P2	P1	P2	P1	P2
z	-2.024	2.254	-2.024	1.879	-2.336	1.879	-3.270	1.127
p	0.043	0.024	0.043	0.060	0.020	0.060	0.001	0.260

Note: Negative and positive z-value indicate a downward and upward trend in the time series, respectively; $p<0.01$ indicates a significance level of 99%.

Table S6. Comparisons of total deposition fluxes of different species between our study in China and two networks in other countries (kg N/S ha^{-1} yr^{-1}).

	Period	RDN	OXN	N	S
USA	1990-2020	2.7	13.3	16.0	16.1
Europe	2000-2019	1.4	4.7	6.1	4.1
China	2005-2020	20.2	15.2	35.4	25.9

Table S7. The ratios of deposition of different forms and species for the six regions as well as eastern (SE+NC with Inner Mongolia excluded), western (NW+TP), and whole China.

Regions		NC	NE	NW	SE	SW	TP	Eastern China	Western China	Whole China
Nitrogen	$R_{dry/wet}$	1.9	2.9	2.5	1.4	2.0	2.6	1.6	2.5	2.3
	$R_{RDN/OXN}$	1.3	1.2	1.4	1.2	1.1	1.7	1.2	1.5	1.3
Sulfur	$R_{dry/wet}$	1.2	1.9	2.4	0.8	1.1	3.7	0.9	2.7	1.8

Table S8. The annual emissions, deposition, and D/E by land use type, according to the latest Land-Use and Land-Cover Change (LUCC) information(http://www.resdc.cn/). "Urban" includes city/town and building categories, and "Rural" includes cropland and countryside categories.

LUCC		Cropland	Forest	Grassland	Water body	City/town	Countryside	Building	Unused land	**Urban**	**Rural**
Emissions (kg N/S ha^{-1} yr^{-1})	NO_X	27.3	8.9	4.5	22.7	86.1	53.8	62.0	1.4	78.7	29.1
	NH_3	22.3	8.8	3.1	11.4	29.3	34.1	20.6	1.1	26.6	23.1
	SO_2	28.2	9.9	5.2	25.0	68.0	44.7	70.9	1.3	68.9	29.3
Deposition (kg N/S ha^{-1} yr^{-1})	Dry OXN	13.1	13.0	8.9	9.9	15.5	14.3	14.2	7.2	15.1	13.2
	Wet OXN	7.4	5.0	3.9	5.7	9.0	8.5	7.5	2.9	8.6	7.5
	Total OXN	20.5	18.0	12.8	15.7	24.5	22.8	21.7	10.2	23.6	20.7
	Dry RDN	16.8	13.8	13.7	14.6	19.1	19.3	17.0	13.8	18.4	17.0
	Wet RDN	8.7	5.8	4.8	7.3	11.2	11.9	10.2	4.6	10.9	8.9
	Total RDN	25.5	19.6	18.5	22.0	30.3	31.2	27.2	18.3	29.3	25.9
	Dry N	29.9	26.8	22.6	24.6	34.5	33.6	31.2	21.0	33.5	30.2
	Wet N	16.1	10.8	8.7	13.0	20.2	20.4	17.7	7.5	19.5	16.4
	Total N	46.0	37.6	31.3	37.6	54.8	54.0	48.9	28.5	53.0	46.6
	Dry S	17.8	17.3	16.0	17.6	17.4	18.0	18.6	16.0	17.8	17.8
	Wet S	14.9	12.9	5.7	10.2	18.1	17.8	16.6	4.0	17.6	15.1
	Total S	32.7	30.2	21.7	27.8	35.5	35.8	35.1	20.1	35.4	32.9
D/E	Dry OXN	0.48	1.46	1.99	0.44	0.18	0.27	0.23	5.26	0.19	0.45
	Wet OXN	0.27	0.56	0.88	0.25	0.10	0.16	0.12	2.14	0.11	0.26
	Total OXN	0.75	2.03	2.87	0.69	0.28	0.42	0.35	7.40	0.30	0.71
	Dry RDN	0.75	1.58	4.34	1.29	0.65	0.57	0.83	12.23	0.69	0.74
	Wet RDN	0.39	0.66	1.52	0.64	0.38	0.35	0.50	4.05	0.41	0.39
	Total RDN	1.15	2.24	5.86	1.93	1.03	0.91	1.32	16.28	1.10	1.12
	Dry S	0.63	1.75	3.10	0.70	0.26	0.40	0.26	12.46	0.26	0.61
	Wet S	0.53	1.30	1.10	0.41	0.27	0.40	0.23	3.14	0.26	0.52
	Total S	1.16	3.05	4.21	1.11	0.52	0.80	0.50	15.61	0.51	1.12

Table S9 in the revised supplement: Comparison of the annual V_d of nitrogen compounds by land use type in this and other studies (cm s^{-1}).

Land use type	Deposition velocity (cm s^{-1})						References
	NO_2	HNO_3	NO_3^-	NH_3	NH_4^+	SO_2	
Farmland	0.17	1.45	0.15	0.43	0.15	0.44	This study
	0.18	1.52	0.19	0.40	0.19		Xu et al. (2015)
	0.10	0.76	0.25	0.18		0.25	Zhang et al. (2004)
						0.56	Zhang et al. (2003)
Urban	0.14	1.37	0.15	0.44	0.15	0.44	This study
	0.06			0.78			Pan et al. (2012)
	0.03					0.20	Su et al. (2012)
						0.55	Zhang et al. (2003)
	0.07	1.77	0.44	0.28	0.44		Li et al. (2013)
	0.30	1.10	0.24	0.50	0.24		Luo et al. (2013)
Coastal	0.16	1.56	0.10	0.65	0.13	0.66	This study
	0.01	0.63		0.63			Zhang et al. (2010)
	0.01	0.84	0.27	0.55	0.27	0.63	Zhang et al. (2004)
						0.40	Su et al. (2012)
Forest	0.19	2.23	0.16	0.41	0.16	0.46	This study
	0.10	2.45	0.30	0.20	0.30		Zhang et al. (2004)
	0.19	2.23	0.16	0.41	0.16		Xu et al. (2015)
	0.04					0.16	Su et al. (2012)
Grassland	0.15	1.09	0.19	0.38	0.19	0.33	This study
	0.13	1.16	0.28	0.23	0.28	0.37	Zhang et al. (2004)
	0.15						Xu et al. (2015)
						0.49	Zhang et al. (2003)

Note: Zhang et al. (2004), Su et al. (2012), Xu et al. (2015), Zhang et al. (2010) and Zhang et al. (2003) applied RegADMS, NAQPMS, GEOS-Chem, MM5/CMAQ and AURAMS, respectively. In particular, Zhang et al (2003) focused on the global land use and did not provide specific discussion for China, and was thus excluded when calculating the mean of China.

Figure S1. Correlations between simulated SO_4^{2-} and SO_2 concentrations from GAM.

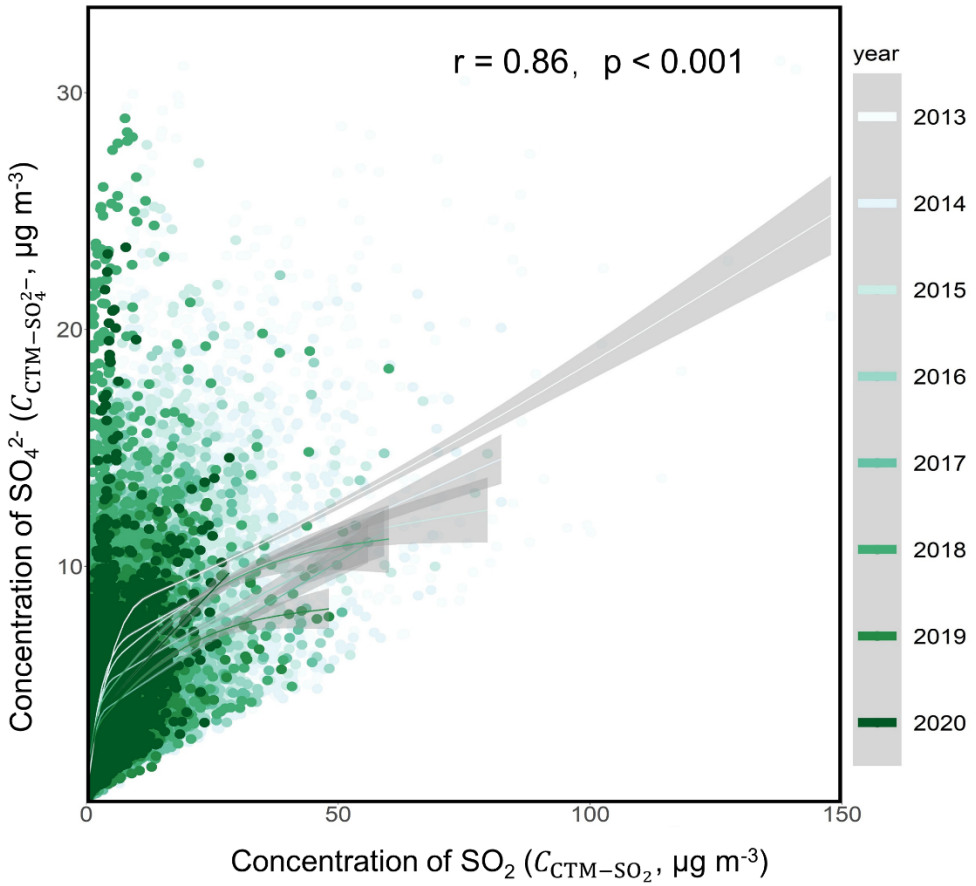

Figure S2. The RF algorithm monthly performance of CNEMC with the 10-fold cross validation. R^2 and RMSE are calculated with equations below the figure (the unit of RMSE are kg N/S ha^{-1} yr^{-1}).

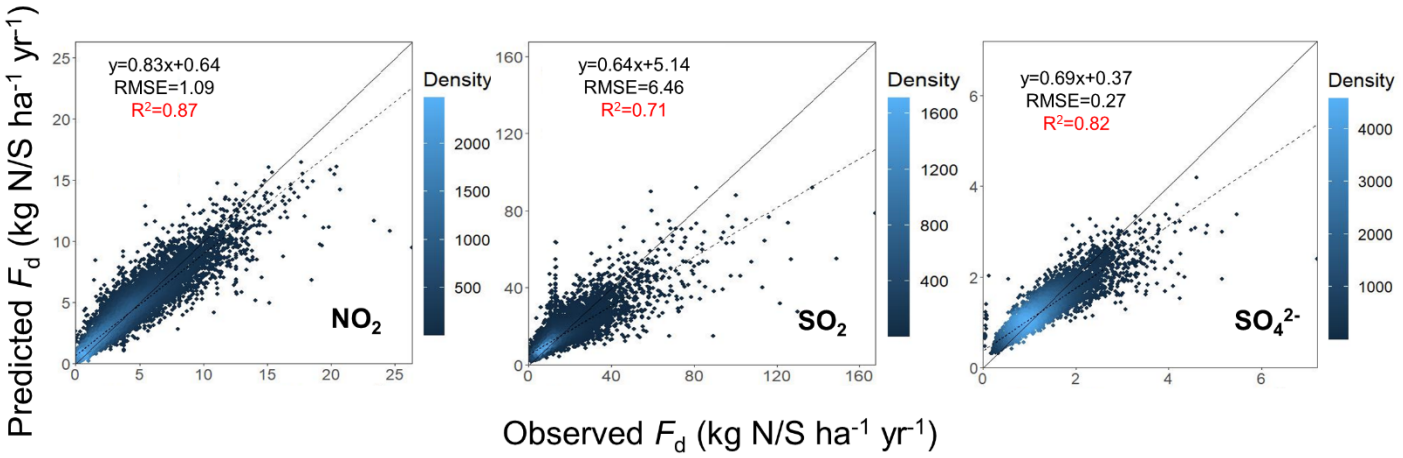

Note: The R^2, RMSE, MPE and RPE were calculated using following equations (*P* and *O* indicates the results from prediction and observation, respectively):

$$R^2 = \frac{\sum_{i=1}^{n}(P_i - \overline{O})^2}{\sum_{i=1}^{n}(O_i - \overline{O})^2}$$

$$\mathrm{RMSE} = \sqrt{\frac{1}{n}\sum_{i=1}^{n}(P_i - O_i)^2}$$

Figure S3. The same as Figure S2 but for NNDMN.

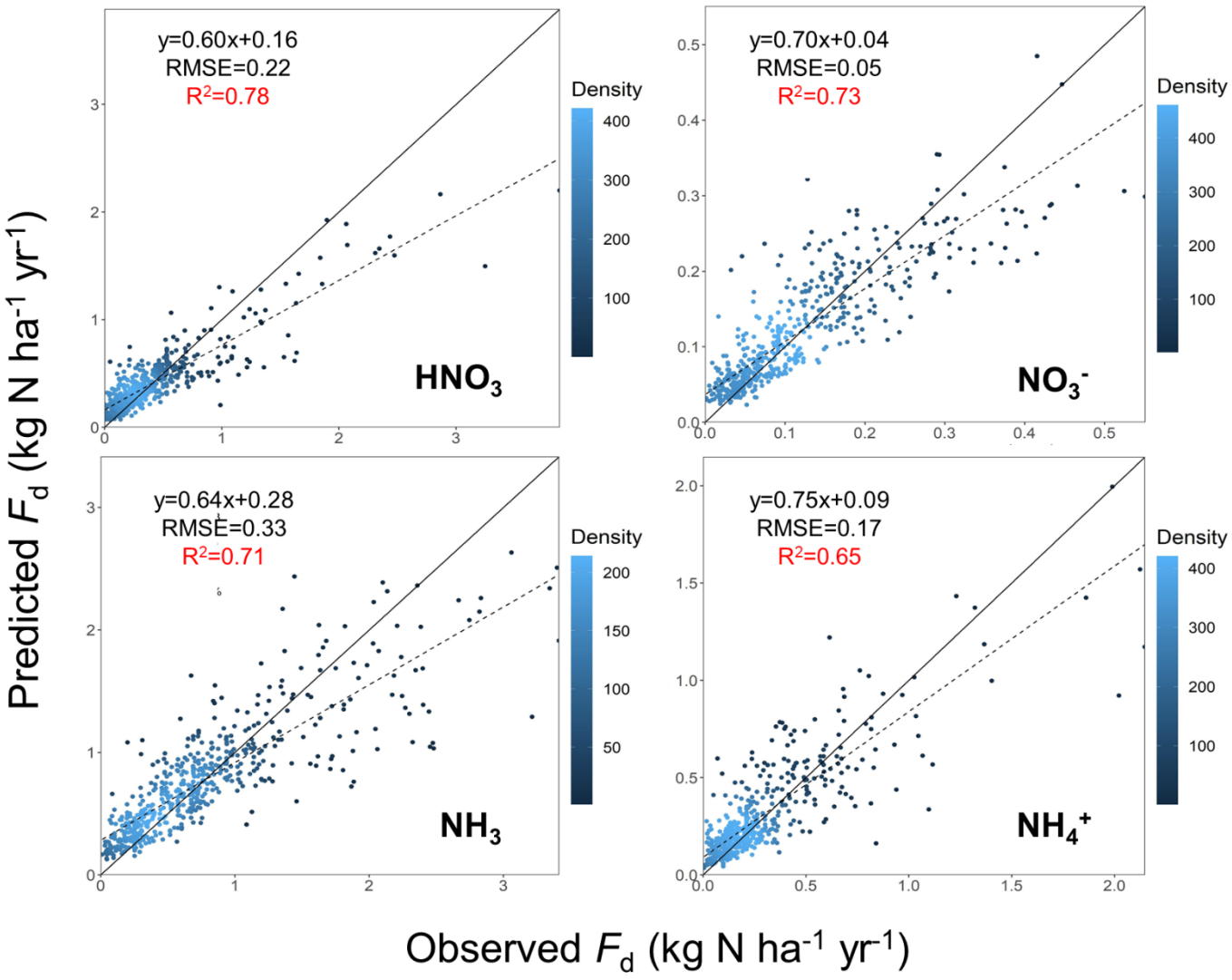

Figure S4. China average total precipitation from ECMWF: https://apps.ecmwf.int/datasets/data/interim-full-daily/levtype=sfc/.

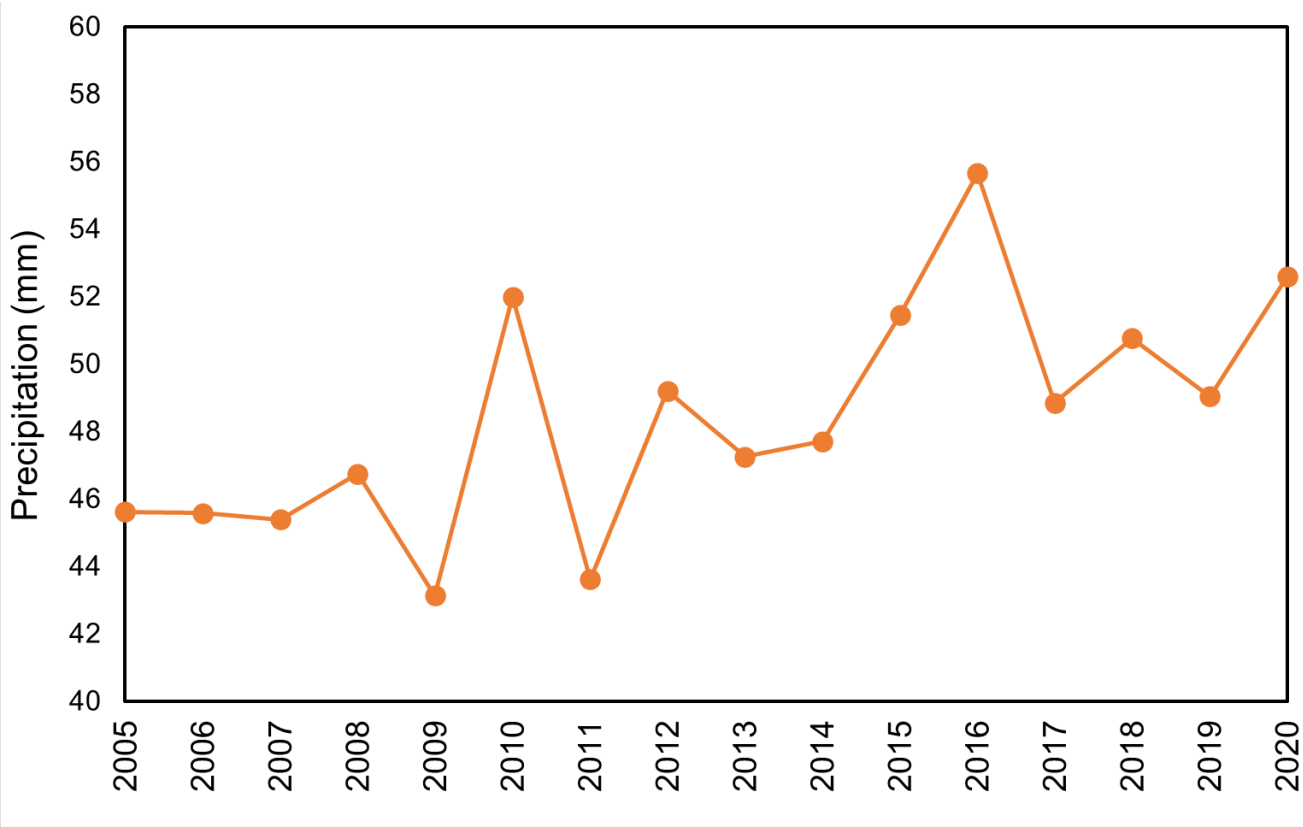

Figure S5. The monthly means of the modeled dry deposition velocity of N and S during 2013-2020.

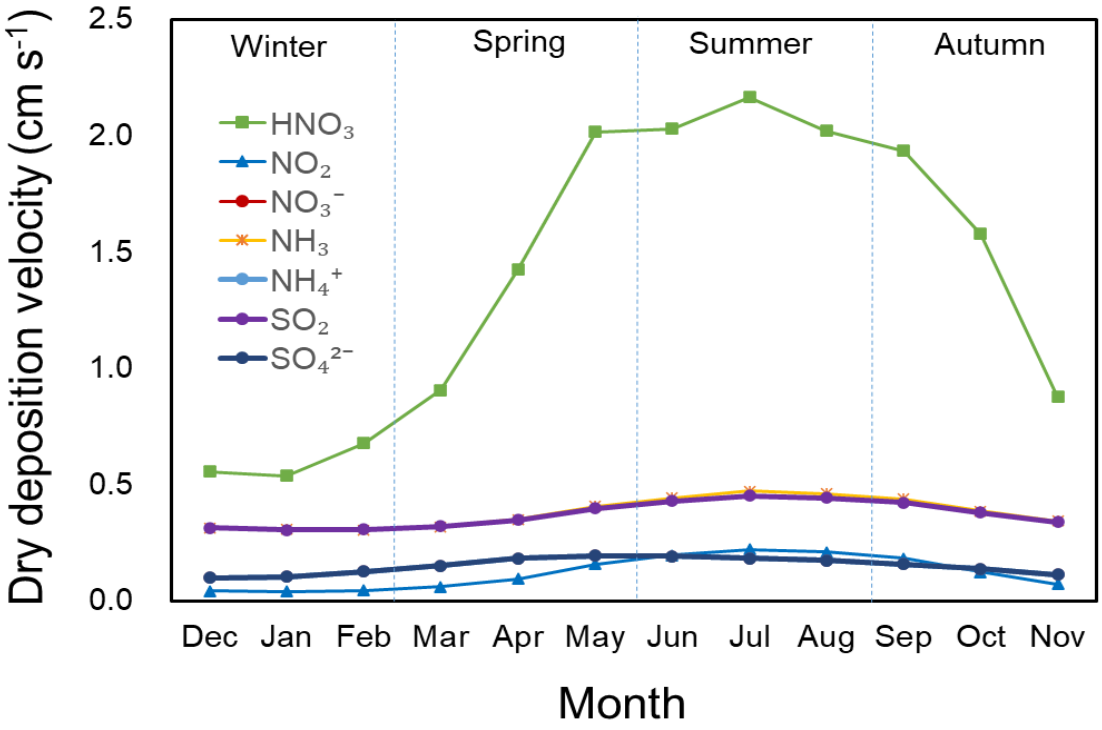

References

Breiman, L.: Random forests, Mach. Learn., 45, 5-32, https://doi.org/10.1023/a:1010933404324, 2001.

Grömping, U.: Variable importance assessment in regression: linear regression versus Random Forest, The American Statistician, 63, 308-319, https://doi.org/10.1198/tast.2009.08199, 2009.

Ge, B. Z., Wang, Z. F., Xu, X. B., Wu, J. B., Yu, X. L., and Li, J.: Wet deposition of acidifying substances in different regions of China and the rest of East Asia: modeling with updated NAQPMS, Environ. Pollut., 187, 10-21, https://doi.org/10.1016/j.envpol.2013.12.014, 2014.

Itahashi, S., Yumimoto, K., Uno, I., Hayami, H., Fujita, S.-i., Pan, Y., and Wang, Y.: A 15-year record (2001–2015) of the ratio of nitrate to non-sea-salt sulfate in precipitation over East Asia, Atmos. Chem. Phys., 18, 2835-2852, https://doi.org/10.5194/acp-18-2835-2018, 2018.

Hicks, B. B., Baldocchi, D. D., Meyers, T. P., Hosker, R. P., and Matt, D. R.: A preliminary multiple resistance routine for deriving dry deposition velocities from measured quantities., Water Air Soil Pollut., 36, 311-330, https://doi.org/https://doi.org/10.1007/BF00229675, 1987.

Jia, Y., Yu, G., Gao, Y., He, N., Wang, Q., Jiao, C., and Zuo, Y.: Global inorganic nitrogen dry deposition inferred from ground- and space-based measurements, Sci. Rep., 6, 19810, https://doi.org/10.1038/srep19810, 2016.

Jia, Y., Yu, G., He, N., Zhan, X., Fang, H., Sheng, W., Zuo, Y., Zhang, D., and Wang, Q.: Spatial and decadal variations in inorganic nitrogen wet deposition in China induced by human activity, Sci. Rep., 4, 3763, https://doi.org/10.1038/srep03763, 2014.

Jiang, W., Zhu, X., Shen, J., Huang, Z., Gong, D., Li, Y., and Wu, J.: Atmospheric sulfur deposition in a paddy rice region in the hilly region in central china, China Environ. Sci., 40, 4848-4856, http://www.zghjkx.com.cn/EN/Y2020/V40/I11/4848, 2020. (in Chinese)

Kuribayashi, M., Ohara, T., Morino, Y., Uno, I., Kurokawa, J.-i., and Hara, H.: Long-term trends of sulfur deposition in East Asia during 1981–2005, Atmos. Environ., 59, 461-475, https://doi.org/10.1016/j.atmosenv.2012.04.060, 2012.

Larssen, T., Duan, L., and Mulder, J.: Deposition and leaching of sulfur, nitrogen and calcium in four forested catchments in China: implications for acidification, Environ. Sci. Technol., 45, 1192-1198, https://doi.org/10.1021/es103426p, 2011.

Li, R., Cui, L., Fu, H., Zhao, Y., Zhou, W., and Chen, J.: Satellite-based estimates of wet ammonium (NH_4-N) deposition fluxes across China during 2011-2016 using a space-time ensemble model, Environ. Sci. Technol., 54, 13419-13428, https://doi.org/10.1021/acs.est.0c03547, 2020.

Li, R., Cui, L., Zhao, Y., Meng, Y., Kong, W., and Fu, H.: Estimating monthly wet sulfur (S) deposition flux over China using an ensemble model of improved machine learning and geostatistical approach, Atmos. Environ., 214, 116884, https://doi.org/10.1016/j.atmosenv.2019.116884, 2019.

Liaw, A. and Wiener, M.: Classification and regression by randomForest, 18-22,

Liu, L., Zhang, X., and Lu, X.: The composition, seasonal variation, and potential sources of the atmospheric wet sulfur (S) and nitrogen (N) deposition in the southwest of China, Environ Sci. Pollut. Res. Int., 23, 6363-6375, https://doi.org/10.1007/s11356-015-5844-1, 2016a.

Liu, L., Zhang, X., Wang, S., Lu, X., and Ouyang, X.: A review of spatial variation of inorganic nitrogen (N) wet deposition in China, PLoS One, 11, e0146051, https://doi.org/10.1371/journal.pone.0146051, 2016b.

Liu, L., Zhang, X., Wang, S., Zhang, W., and Lu, X.: Bulk sulfur (S) deposition in China, Atmos. Environ., 135, 41-49, https://doi.org/10.1016/j.atmosenv.2016.04.003, 2016c.

Liu, L., Yang, Y., Xi, R., Zhang, X., Xu, W., Liu, X., Li, Y., Liu, P., and Wang, Z.: Global wet-reduced nitrogen deposition derived from combining satellite measurements with output from a chemistry transport model, J. Geophys. Res., 126, https://doi.org/10.1029/2020jd033977, 2021.

Liu, L., Zhang, X., Xu, W., Liu, X., Lu, X., Chen, D., Zhang, X., Wang, S., and Zhang, W.: Estimation of monthly bulk nitrate deposition in China based on satellite NO_2 measurement by the Ozone Monitoring Instrument, Remote Sens. Environ., 199, 93-106, https://doi.org/10.1016/j.rse.2017.07.005, 2017a.

Liu, L., Zhang, X., Zhang, Y., Xu, W., Liu, X., Zhang, X., Feng, J., Chen, X., Zhang, Y., Lu, X., Wang, S., Zhang, W., and Zhao, L.: Dry particulate nitrate deposition in China, Environ. Sci. Technol., 51, 5572-5581, https://doi.org/10.1021/acs.est.7b00898, 2017b.

Luo, X., Pan, Y., Goulding, K., Zhang, L., Liu, X., and Zhang, F.: Spatial and seasonal variations of atmospheric sulfur concentrations and dry deposition at 16 rural and suburban sites in China, Atmos. Environ., 146, 79-89, https://doi.org/10.1016/j.atmosenv.2016.07.038, 2016.

Lye, C. and Tian, H.: Spatial and temporal patterns of nitrogen deposition in China: Synthesis of observational data, J. Geophys. Res., 112, https://doi.org/10.1029/2006jd007990, 2007.

Nowlan, C. R., Martin, R. V., Philip, S., Lamsal, L. N., Krotkov, N. A., Marais, E. A., Wang, S., and Zhang, Q.: Global dry deposition of nitrogen dioxide and sulfur dioxide inferred from space-based measurements, Global Biogeochem. Cycles, 28, 1025-1043, https://doi.org/10.1002/2014gb004805, 2014.

Pan, Y. P., Wang, Y. S., Tang, G. Q., and Wu, D.: Wet and dry deposition of atmospheric nitrogen at ten sites in Northern China, Atmos. Chem. Phys., 12, 6515-6535, https://doi.org/10.5194/acp-12-6515-2012, 2012.

Pan, Y. P., Wang, Y. S., Tang, G. Q., and Wu, D.: Spatial distribution and temporal variations of atmospheric sulfur deposition in Northern China: insights into the potential acidification risks, Atmos. Chem. Phys., 13, 1675-1688, https://doi.org/10.5194/acp-13-1675-2013, 2013.

Qiao, X., Xiao, W., Jaffe, D., Kota, S. H., Ying, Q., and Tang, Y.: Atmospheric wet deposition of sulfur and nitrogen in Jiuzhaigou National Nature Reserve, Sichuan Province, China, Sci. Total Environ., 511, 28-36, https://doi.org/10.1016/j.scitotenv.2014.12.028, 2015a.

Qiao, X., Tang, Y., Hu, J., Zhang, S., Li, J., Kota, S. H., Wu, L., Gao, H., Zhang, H., and Ying, Q.: Modeling dry and wet deposition of sulfate, nitrate, and ammonium ions in Jiuzhaigou National Nature Reserve, China using a source-oriented CMAQ model: Part I. Base case model results, Sci. Total Environ., 532, 831-839, https://doi.org/10.1016/j.scitotenv.2015.05.108, 2015b.

Su, H., Yin, Y., Zhu, B., Wang, Z., Li, J., and Pan, X.: Numerical simulation and sensitive factors analyse for dry deposition of SO_2 and NO_2 in Bohai Rim area of China, China Environ. Sci., 32, 1921-1932, 2012.

Tan, J., Su, H., Itahashi, S., Tao, W., Wang, S., Li, R., Fu, H., Huang, K., Fu, J. S., and Cheng, Y.: Quantifying the wet deposition of reactive nitrogen over China: Synthesis of observations and models, Sci. Total Environ., 851, 158007, https://doi.org/10.1016/j.scitotenv.2022.158007, 2022.

Walcek, C. J., Brost, R. A., Chang, J. S., and Wesely, M. L.: SO_2, sulfate and HNO_3 deposition velocities computed using regional landuse and meteorological data, Atmos. Environ., 20, 949-964, https://doi.org/10.1016/0004-6981(86)90279-9, 1986.

Wei, J., Li, Z., Guo, J., Sun, L., Huang, W., Xue, W., Fan, T., and Cribb, M.: Satellite-derived 1-km-resolution PM_1 concentrations from 2014 to 2018 across China, Environ. Sci. Technol., 53, 13265-13274, https://doi.org/10.1021/acs.est.9b03258, 2019.

Wen, Z., Xu, W., Li, Q., Han, M., Tang, A., Zhang, Y., Luo, X., Shen, J., Wang, W., Li, K., Pan, Y., Zhang, L., Li, W., Collett, J. L., Jr., Zhong, B., Wang, X., Goulding, K., Zhang, F., and Liu, X.: Changes of nitrogen deposition in China from 1980 to 2018, Environ. Int., 144, 106022, https://doi.org/10.1016/j.envint.2020.106022, 2020.

Wesely, M. L.: Parameterization of surface resistances to gaseous dry deposition in regional-scale numerical models, Atmos. Environ., 23, 1293-1304, https://doi.org/https://doi.org/10.1016/0004-6981(89)90153-4, 1989.

Xu, W., Zhang, L., and Liu, X.: A database of atmospheric nitrogen concentration and deposition from the nationwide monitoring network in China, Sci. Data, 6, 51, https://doi.org/10.1038/s41597-019-0061-2, 2019.

Xu, W., Luo, X. S., Pan, Y. P., Zhang, L., Tang, A. H., Shen, J. L., Zhang, Y., Li, K. H., Wu, Q. H., Yang, D. W., Zhang, Y. Y., Xue, J., Li, W. Q., Li, Q. Q., Tang, L., Lu, S. H., Liang, T., Tong, Y. A., Liu, P., Zhang, Q., Xiong, Z. Q., Shi, X. J., Wu, L. H., Shi, W. Q., Tian, K., Zhong, X. H., Shi, K., Tang, Q. Y., Zhang, L. J., Huang, J. L., He, C. E., Kuang, F. H., Zhu, B., Liu, H., Jin, X., Xin, Y. J., Shi, X. K., Du, E. Z., Dore, A. J., Tang, S., Collett, J. L., Goulding, K., Sun, Y. X., Ren, J., Zhang, F. S., and Liu, X. J.: Quantifying atmospheric nitrogen deposition through a nationwide monitoring network across China, Atmos. Chem. Phys., 15, 12345-12360, https://doi.org/10.5194/acp-15-12345-2015, 2015.

Yu, G., Jia, Y., He, N., Zhu, J., Chen, Z., Wang, Q., Piao, S., Liu, X., He, H., Guo, X., Wen, Z., Li, P., Ding, G., and Goulding, K.: Stabilization of atmospheric nitrogen deposition in China over the past decade, Nature Geosci., 12, 424-431, https://doi.org/10.1038/s41561-019-0352-4, 2019.

Yu, H., He, N., Wang, Q., Zhu, J., Xu, L., Zhu, Z., and Yu, G.: Wet acid deposition in Chinese natural and agricultural ecosystems: Evidence from national-scale monitoring, J. Geophys. Res.: Atmospheres, 121, 10,995-911,005, https://doi.org/10.1002/2015jd024441, 2016.

Zhang, B., Li, Z., Feng, Q., Gui, J., Zhao, Y., and Zhang, B.: Environmental significance of atmospheric nitrogen deposition in the transition zone between the Tibetan Plateau and arid region, Chemosphere, 307, 136096, https://doi.org/10.1016/j.chemosphere.2022.136096, 2022.

Zhang, L., Gong, S., Padro, J., and Barrie, L.: A size-segregated particle dry deposition scheme for an atmospheric aerosol module, Atmos. Environ., 35, 549-560, 2001.

Zhang, L., Brook, J. R., and Vet, R.: Evaluation of a non-stomatal resistance parameterization for SO_2 dry deposition, Atmos. Environ., 37, 2941-2947, https://doi.org/10.1016/s1352-2310(03)00268-1, 2003.

Zhang, X. Y., Lu, X. H., Liu, L., Chen, D. M., Zhang, X. M., Liu, X. J., and Zhang, Y.: Dry deposition of NO_2 over China inferred from OMI columnar NO_2 and atmospheric chemistry transport model, Atmos. Environ., 169, 238-249, https://doi.org/10.1016/j.atmosenv.2017.09.017, 2017.

Zhang, Y., Wang, T. J., Hu, Z. Y., and Xu, C. K.: Temporal variety and spatial distribution of dry deposition velocities of typical air pollutants over different land-use types, Climatic Environ. Res., 9, 591-604, 2004. (In Chinese)

Zhao, Y., Zhang, L., Chen, Y., Liu, X., Xu, W., Pan, Y., and Duan, L.: Atmospheric nitrogen deposition to China: A model analysis on nitrogen budget and critical load exceedance, Atmos. Environ., 153, 32-40, https://doi.org/10.1016/j.atmosenv.2017.01.018, 2017.

Zhou, K., Zhao, Y., Zhang, L., and Xi, M.: Declining dry deposition of NO_2 and SO_2 with diverse spatiotemporal patterns in China from 2013 to 2018, Atmos. Environ., 262, 118655, https://doi.org/10.1016/j.atmosenv.2021.118655, 2021.

Zhu, J., He, N., Wang, Q., Yuan, G., Wen, D., Yu, G., and Jia, Y.: The composition, spatial patterns, and influencing factors of atmospheric wet nitrogen deposition in Chinese terrestrial ecosystems, Sci. Total Environ., 511, 777-785, https://doi.org/10.1016/j.scitotenv.2014.12.038, 2015.